scientific reports

Check for updates

OPEN

Effective dynamic energy management algorithm for grid-interactive microgrid with hybrid energy storage system

Yaya Kamagaté[1]✉ & Heli Amit Shah[2]

Microgrids offer an optimistic solution for delivering electricity to remote regions and incorporating renewable energy into existing power systems. However, the energy balance between generation and consumption remains a significant challenge in microgrid setups. This research presents an adaptive energy management approach for grid-interactive microgrids. The DC microgrid is established by combining solar PV with a battery-supercapacitor (SC) hybrid energy storage system (HESS). The proposed approach integrates the frequency separation strategy with a rule-based algorithm to ensure optimal power sharing among sources while maintaining the safe operation of storage units. Specifically, the battery meets steady-state energy demands, the SC addresses transient power requirements, and the grid support is tailored to system needs. The method employs the dq reference frame technique to control the grid inverter (VSC). The key merits include efficient power allocation, fast regulation of the DC link voltage irrespective of load or generation variations, seamless transition between scenarios, and introduction of a straightforward battery state of charge (SOC)-based coefficient for allocating power between the battery and the grid while enhancing the power quality within the grid. Moreover, safety measures prevent the SC from overcharging, the battery from high current, overcharging, and deep discharging, potentially extending their lifespan. Validation and implementation of the method are conducted using MATLAB/Simulink.

Keywords Energy management, Grid-interactive microgrid, Power allocation, SOC, Storage units

The future of the electrical power system is heavily reliant on renewable energy resources and distributed generation, driven by global energy demand, environmental concerns, and constrained availability of traditional energy sources. However, the intermittency and unpredictability of commonly used renewable energy sources such as solar PV and wind pose a challenge. Therefore, incorporating energy storage elements is crucial for a reliable and continuous electricity supply[1,2]. Battery energy storage, the leading technology for solar PV-based microgrids, effectively addresses the challenge of renewable energy intermittency[3–5]. However, batteries degrade faster when handling transient power demand[6].

Combining a battery with another energy storage device that can handle the transient power demand can solve the above-stated problem[7,8]. That is known as a hybridization of storage units. Ideally, the concept consists of using one high-power device to handle transient power demand and one high-energy device for the average energy requirement. Several storage combinations have been used in the literature for various applications[9–12]. Among these combinations, the couple battery-SC has gained notable attention[13,14]. In the couple battery-SC, the battery handles the slow energy requirement while the SC manages the fluctuating power demand. When merging multiple storage units, power management, and control strategy are critical for using complementing qualities and efficiently distributing and controlling the power flow between microgenerators while ensuring the safe operation of storage units[15]. For storage units, this involves prolonging their lifespan by avoiding premature degradation. Hence, the battery must avoid high currents, overcharging, and deep discharging, whereas the SC should be prevented from overcharging[16]. Various methods have been suggested in the literature, from conventional or classical methods such as filtration-based control (FBC) and rule-based control (RBC) to intelligent methods.

[1]Electrical Engineering Department, Parul University, Vadodara, India. [2]Robotics and Automation Engineering Department, Parul University, Vadodara, India. ✉email: 200300418001@paruluniversity.ac.in

In Ref.[17], a strategy for managing energy in a mobile hospital is proposed. An efficient energy management algorithm is developed to control the power converters and manage the continuous energy flow between the hybrid power system's components and the mobile hospital load. The loads are classified by priority, the DC bus voltage is successfully kept constant, and the storage devices' SOCs are made to work within safe limits. However, loads must be disconnected based on the battery's SOC, which can lead to critical situations and create hazardous environments for patients and staff. This may result in interrupted medical treatments, compromised life-support systems, and an unsafe working environment for healthcare professionals.

In Ref.[18], an active distribution system's energy management and voltage control is suggested, with a PV-battery-SC-diesel generator (DG) microgrid configuration that operates in islanded and grid-connected modes. The method employs a HESS to extract maximum power from PV while preventing the DG from sudden loading. This reduces maintenance concerns and running costs and ensures fuel-efficient operation of the DG. The proposed power management system is tested under various situations, including DG failure and extreme conditions without a DG. However, using a diesel generator to support the DC microgrid can contribute to carbon emissions.

Reference[19] introduces a military microgrid's power flow control technique. The technique increases the battery's lifetime, controls the SC's current, and overcomes SC overcharge to keep the system running when it is drained to its lower operational limit. The study provides a sensitivity analysis by linking the HESS control technique and configuration to the system's economics by examining the annualized cash flow. However, the current gain parameter is crucial for the SC's ability to switch between discharging and charging modes.

The approach in Ref.[20] proposed a HESS-based control and energy management method for multiple operational scenarios. Using a 4th-order polynomial equation, the proposed control effectively distributes power among various sources, regulates the DC link voltage irrespective of generation or load changes, and reduces the battery discharging/charging rate during transient power variation.

Reference[21] presents a joint and conceptual strategy for designing and controlling a hybrid renewable energy system with a HESS. The control approach achieves appropriate power balancing and improves dynamic response, DC bus voltage stability, and load voltage/frequency under different weather and load interruption scenarios. However, the battery's and SC's SOC levels are not considered, which may result in premature degradation of storage units.

Reference[22] suggests an optimal energy management strategy for offshore wind/marine current/battery/SC hybrid renewable system. The suggested control algorithm demonstrates the system's ability to minimize power loss and voltage fluctuations while managing the charge and discharge states of the battery and ultracapacitor (UC). The proposed algorithm continuously transfers the required power across the hybrid energy storage system to meet load demands consistently. However, the method overlooks the UC's SOC level, which may result in insufficient UC power for future needs.

In Ref.[23], a PV/HESS-based distributed rule-based power management technique with an active compensation technique is proposed. The active compensation technique enhances power smoothing efficiency, reduces SC size, and reduces computational complexity, making it suitable for real-time applications. Additionally, a distributed supervisory control strategy and hybrid dynamic adaptive filter ensure the HESS's reliable operation and scalability, with agents modeled in a hybrid dynamical framework for efficient control. However, computational complexity still appears, and deactivating the power smoothing filter to regulate SC SOC may result in high-frequency current being allocated to the battery, which may increase battery stress and reduce its lifetime.

A summary of classical energy management methods is given in Table 1.

The literature also reports the utilization of intelligent methods like artificial neural networks (ANN)[24–26], model predictive control (MPC)[27–29], fuzzy logic control (FLC)[30–32], etc., to address the limits of classical methods. However, ANN results depend on training data, MPC requires complex mathematical formulations and high computational burdens, and fuzzy logic's real-time implementation is challenging.

To address the abovementioned issues, this paper presents a new and straightforward energy management approach. The method introduces a simple linear battery SOC-based power allocation coefficient for effectively distributing power between the battery and the grid. The proposed scheme is designed to mitigate the intermittence under different operating scenarios, ensure appropriate power flow between sources, regulate the DC bus voltage regardless of the load or generation changes, safely operate the battery and SC, and ensure a seamless transition between operating conditions and scenarios. Moreover, the simplicity of the method enhances its suitability for real-world setups.

The remainder of the paper is structured as follows: Sect. "System configuration" outlines the system configuration. Section "Energy management and control strategies" elucidates the energy management and control strategies. Section "Results and discussion" displays and analyzes the simulation results. The final section offers concluding remarks.

System configuration

The microgrid configuration under study, shown in Fig. 1, includes a PV source, battery storage, SC storage, and the grid. The PV source is interfaced by a DC-DC boost converter, controlled by the incremental conductance (InCond) maximum power point tracking (MPPT) algorithm, and linked to the DC bus. The battery and SC are connected to the DC link through a bidirectional DC-DC buck-boost converter, enabling bidirectional power flow between the DC bus and the storage units. A three-phase VSC links the DC link to the utility grid. The VSC can act as an inverter or rectifier based on system requirements. The loads are a single-phase DC load and a three-phase AC load.

Refs.	HESS	Microgrid	Control technique	Key merits	Limitations
[17]	Battery/ SC	PV/diesel generator/ battery/SC (islanded and grid-connected)	FBC	The proposed algorithm manages the continuous energy flow between the hybrid power system's components and the mobile hospital load. The DC bus voltage is constant, and the storage devices' SOCs work within safe limits. The method can help improve patient treatment in remote states.	Loads' disconnection based on the battery's State of Charge (SOC) may result in interrupted medical treatments, compromised life-support systems, and an unsafe working environment for healthcare professionals.
[18]	Battery/ SC	PV/diesel generator/ battery/SC (islanded and grid-connected)	FBC	The proposed strategy prevents the diesel generator (DG) from sudden loading, which reduces maintenance concerns and running costs and ensures the DG's fuel-efficient operation. The method is successfully tested under various situations, including DG failure and extreme conditions without a DG.	Using a diesel generator to support the DC microgrid may contribute to carbon emissions.
[19]	Battery/ SC	PV/battery/SC (remote military)	FBC	The proposed technique increases the battery's lifetime, controls the SC's current, and overcomes SC overcharge to keep the system running when it is drained to its lower operational limit. The method links the HESS control parameters and the annual cash flow.	SC's ability to switch between discharging and charging modes highly depends on the current gain setting.
[20]	Bat/SC	PV/battery/SC (grid-connected)	FBC	The proposed method effectively distributes power among various sources, regulates the DC link voltage irrespective of generation or load changes, and reduces the battery discharging/charging rate during transient power variation.	Delays and failures in communication may prevent the system from operating normally.
[21]	Bat/SC	PV/Wind/ battery/SC (off-grid)	RBC	The control strategy achieves appropriate power balancing and improves dynamic response, DC bus voltage stability, and load voltage/frequency under different weather and load interruption scenarios.	Storage devices' SOCs are not regulated, which could lead to their premature degradation.
[22]	Bat/UC	Wind/marine current /battery/UC (offshore)	RBC	The suggested algorithm demonstrates the system's ability to minimize power loss and voltage fluctuations while managing the charge and discharge states of the battery and ultracapacitor (UC). The method continuously transfers the required power across the HESS to meet load demands consistently.	UC's SOC level is not considered, which may result in insufficient UC power for future needs.
[23]	Bat/SC	PV/battery/SC (on-grid)	RBC	The proposed method enhances power smoothing efficiency, reduces SC size, and reduces computational complexity, making it suitable for real-time applications. Additionally, a distributed supervisory control strategy and hybrid dynamic adaptive filter ensure the HESS's reliable operation and scalability, with agents modeled in a hybrid dynamical framework for efficient control.	Computational complexity and high-frequency current allocated to the battery may increase battery stress and reduce its lifetime.

Table 1. Comparison of classical energy management techniques.

Energy management and control strategies

PV source control

The widely adopted InCond MPPT algorithm is employed to maximize power extraction from the PV source[33]. This method involves comparing actual and previous PV voltage and current values and adjusting (increasing or decreasing) the reference duty cycle accordingly. It is straightforward, and the PV source voltage and current are the only inputs required for maximum power extraction.

DC link voltage control and reference currents generation for storage units and the grid

The overall proposed control strategy is depicted in Fig. 2. The microgrid is designed to uphold a power equilibrium between generation and consumption at any instant, regardless of the operating conditions and scenarios, consequently keeping the DC link voltage constant. The following equation expresses this principle:

$$P_{pv}(t) + P_{bat}(t) + P_{sc}(t) + P_g(t) = P_{tl}(t), \quad (1)$$

where, $P_{pv}(t)$, $P_{bat}(t)$, $P_{sc}(t)$, $P_g(t)$, and $P_{tl}(t)$ are instantaneous PV power, battery power, supercapacitor power, grid power, and total load power, respectively.

Taking into account that the total load (DC load and AC load) comprises the average and the transient demand to be absorbed or released by the battery, the SC, and the grid, (1) can be reformulated to obtain (2).

$$P_{td}(t) = P_{pv}(t) - (P_{acl}(t) + P_{dcl}(t)) = P_{bat}(t) + P_{sc}(t) + P_g(t) = P_{av}(t) + P_{tr}(t), \quad (2)$$

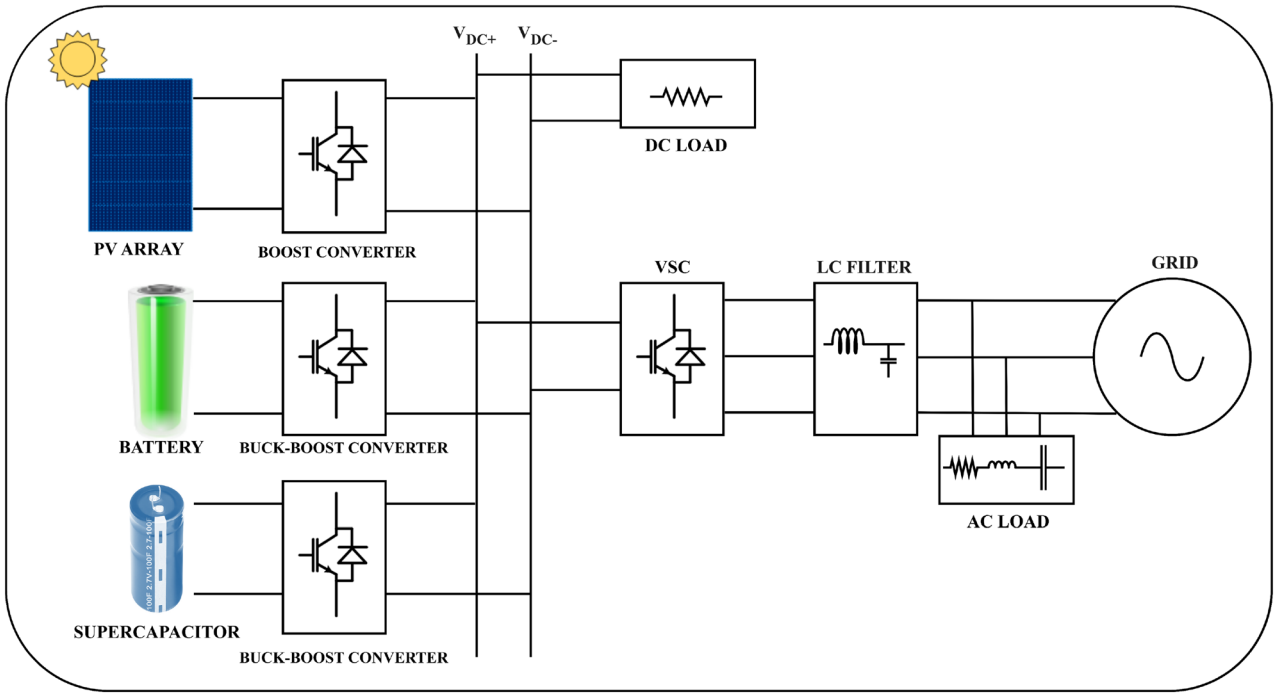

Fig. 1. Proposed microgrid configuration.

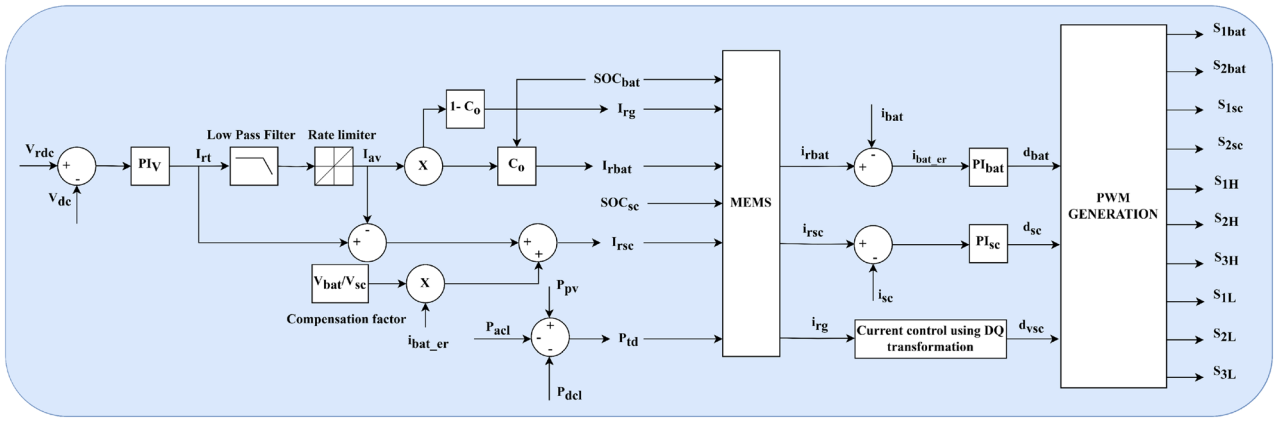

Fig. 2. Overall control strategy.

where, $P_{td}(t)$, $P_{acl}(t)$, $P_{dcl}(t)$, $P_{av}(t)$, and $P_{tr}(t)$ denote, respectively, total power demand, AC load power, DC load power, average power demand, and transient power demand.

The strategy for managing the DC link voltage and generating reference currents for storage units and the grid employs the filtration-based approach[16]. The total reference current (I_{rt}) is obtained from the voltage regulation loop as given by Eq. (3):

$$I_{rt}(s) = \left(K_{P_V} + \frac{K_{I_V}}{s}\right)(V_{rdc} - V_{dc}), \tag{3}$$

where K_{P_V} and K_{I_V} represent the PI controller (PI_V) parameters for the voltage control loop, whereas V_{rdc} and V_{dc} are reference and actual DC bus voltages.

By utilizing a first-order low pass filter (LPF), I_{rt} is segregated into two parts: a low-frequency component (average) and a high-frequency component (transient). The following equation expresses this segregation:

$$I_{av}(s) = \frac{1}{1 + s.T} I_{rt}(s) \tag{4}$$

where I_{av}, and T are the average current and the LPF time constant, respectively.

Employing the suggested linear power allocation coefficient (C_o) shown in Fig. 3, the battery and the grid share the average current while the SC handles the transient current. The battery (I_{rbat}), the SC (I_{rsc}), and the grid (I_{rg}) reference currents are as follows:

$$I_{rbat}(s) = C_o.I_{av}(s), \tag{5}$$

$$I_{rg}(s) = (1 - C_o).I_{av}(s), \tag{6}$$

$$I_{rsc}(s) = \left(1 - \frac{1}{1+sT}\right).I_{rt}(s) + \frac{V_{bat}}{V_{sc}} * I_{bat\_er} \tag{7}$$

where V_{bat}, V_{sc}, and I_{bat_er} stand for the battery voltage, the SC voltage, and the battery current error. The supplementary term appearing in SC current is used to overcome the slow response of the battery.

The proposed power allocation coefficient is obtained using the following equation in MATLAB software:

$$C_o = \text{subplus}(0.01109375*(SOC_{bat}) - 0.1109375) \tag{8}$$

PI_{bat} and PI_{sc} generate the pulse signals for the battery and the SC after comparing their actual currents (i_{bat} and i_{sc}) to their generated reference currents (i_{rbat} and i_{rsc}).

VSC control

Figure 4 depicts the VSC control method. The method uses a vector control strategy in which the VSC current (I_{abc}) controls the exchange of active and reactive power between the DC microgrid and the grid. The Park transformation decomposes the three-phase abc coordinates (I_{abc}) into dq coordinates (i_d and i_q). The reference phase angle (Θ) for the I_{abc} transformation is derived using the phase-locked loop (PLL) technique. The resultant currents are compared with their reference values (i_{dr} and i_{qr}), and the error signals are fed into the proportional-integral controllers to generate dq reference voltages (V_{dr} and V_{qr}). Subsequently, the inverse Park transformation is employed to derive reference 3-phase voltages (V_{ar}, V_{br}, and V_{cr}) for generating switching pulses for the VSC. In the dq reference frame, the power exchange between the AC and DC subsystems is controlled by i_d (for the active power) and i_q (for the reactive power). The proposed strategy aims to send only active power to the grid. Therefore, the reference current for the q-axis is set to zero ($i_{qr} = 0$). Conversely, the reference current for the d-axis equals the current received from the DC subsystem, thus controlling the DC bus voltage.

Master energy management system (MEMS)

The MEMS is vital for adequate power flow between the sources and the loads. It collects information from the sources and loads and makes appropriate decisions to ensure adequate power management. The MEMS flowchart is shown in Fig. 5. Two (2) scenarios are envisaged, depending on total power demand (P_{td}). Each scenario has four (4) cases depending on the SOCs of the storage units.

Surplus power scenario (SPS)

Here, the PV power surpasses the total load power (i.e. P_{td} is positive). The surplus power is utilized to charge the storage units. Depending on SOC levels and total power demand, this surplus power can also be sent to the

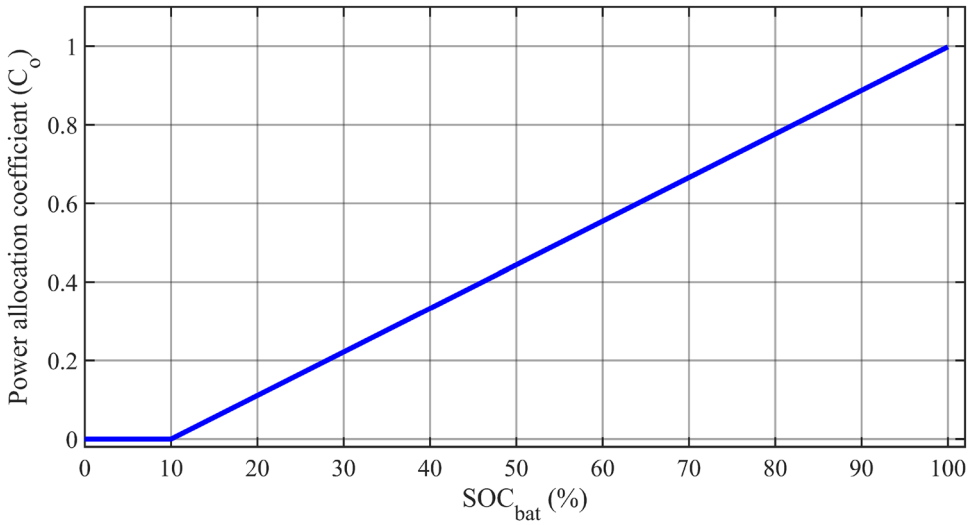

Fig. 3. Proposed power allocation coefficient.

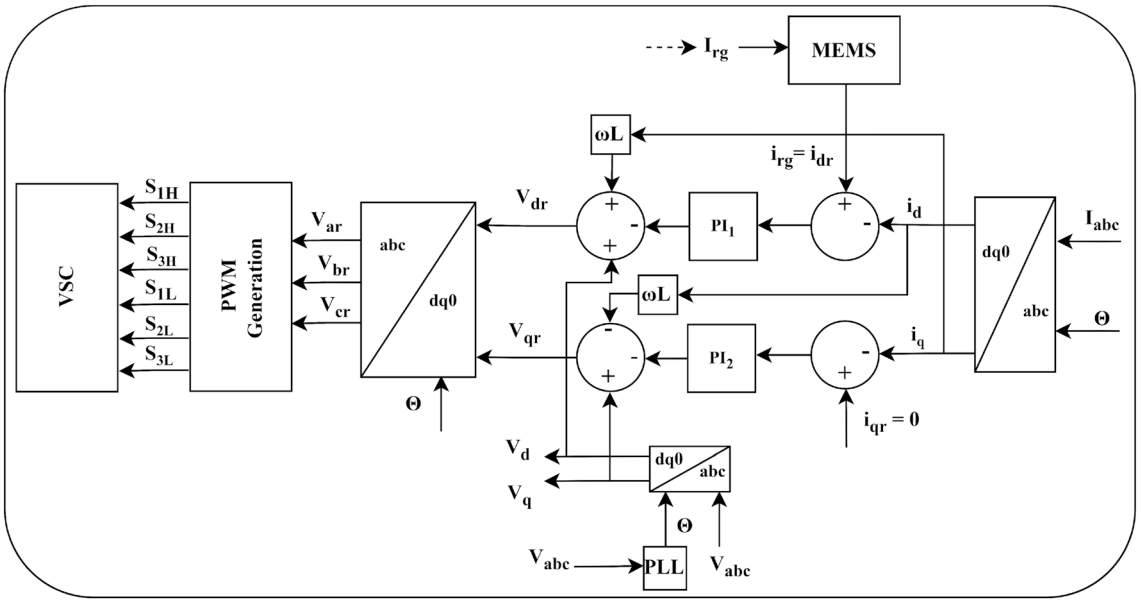

Fig. 4. VSC control block diagram.

grid. Table 2, details the different cases and the corresponding actions and currents. I_{batr} (battery) and I_{scr} (SC) represent the rated charging current of the storage units.

Deficit power scenario (DPS)
In this scenario, the PV power falls short of the total load power (i.e. P_{td} is negative). The deficit power to be supplied to the loads is divided between the storage units and the grid. C_o is introduced, and SOC levels of storage devices are used to allocate power. The cases and corresponding actions and currents are given in Table 3.

Results and discussion

All system components were methodically prepared for the simulation, utilizing MATLAB/Simulink. The scenario chosen involves fluctuating solar irradiance conditions while maintaining a constant temperature of 25 °C. Figure 6 provides a visual representation of the solar irradiance profiles. The design parameters for the system are found in Table 4. The proposed system is evaluated for three scenarios: (1) surplus power scenario (SPS), (2) deficit power scenario (DPS), and (3) transition scenario (TS).

Surplus power scenario (SPS)

Figure 7 highlights the results for SPS. The total load remains constant. At the same time, the solar irradiance varies according to the pattern indicated in Fig. 6 (SPS). The PV power is maintained significantly higher than the total load power, and the SOC values are set.

During the initial phase (0 to 2 s), the extra PV power is utilized to charge the storage units at their rated charging current, and the remaining power is transferred to the grid ($P_g < 0$).

The solar irradiance drops at t = 2s and t = 4s, decreasing the PV power and causing a DC bus voltage deviation. Consequently, the SC reacts by supplying the transient demand, and the grid supplies the average power, keeping the DC bus voltage constant. At the same time, the battery and the SC continue charging.

In the interval (5 to 6 s), SOC_{bat} reaches its maximum safety limit (90%), as shown in Fig. 7c. To prevent it from overcharging, the battery current becomes zero. The SC reacts to this transient phenomenon by absorbing the transient power while the grid handles the average part.

At t = 6s, an increase in solar irradiance boosts the PV power, resulting in another DC bus voltage deviation. SOC_{bat} has already reached its maximum safety limit, so the battery has not taken action. The SC absorbs the transient power, and the grid absorbs the average power, maintaining the DC bus voltage constant. The SC charges, and the grid receives power ($P_g < 0$).

In the interval time (7 to 8 s), SOC_{sc} reaches its maximum level (95%), as depicted in Fig. 7d. SC charging current is nullified to avoid SC overcharging. The storage units have now hit their maximum safety limits.

Another increase in solar irradiance is observed at t = 8s. As the storage units have reached their maximum safety limits, the grid fulfills the system transient requirement to maintain the DC bus voltage constant while PV extra power is transferred to the grid.

Regardless of the case, the DC bus voltage is kept at 700 V, the frequency is maintained at 50 Hz, and the grid's unity power factor is maintained, as seen in (e), (f), (h), Fig. 7.

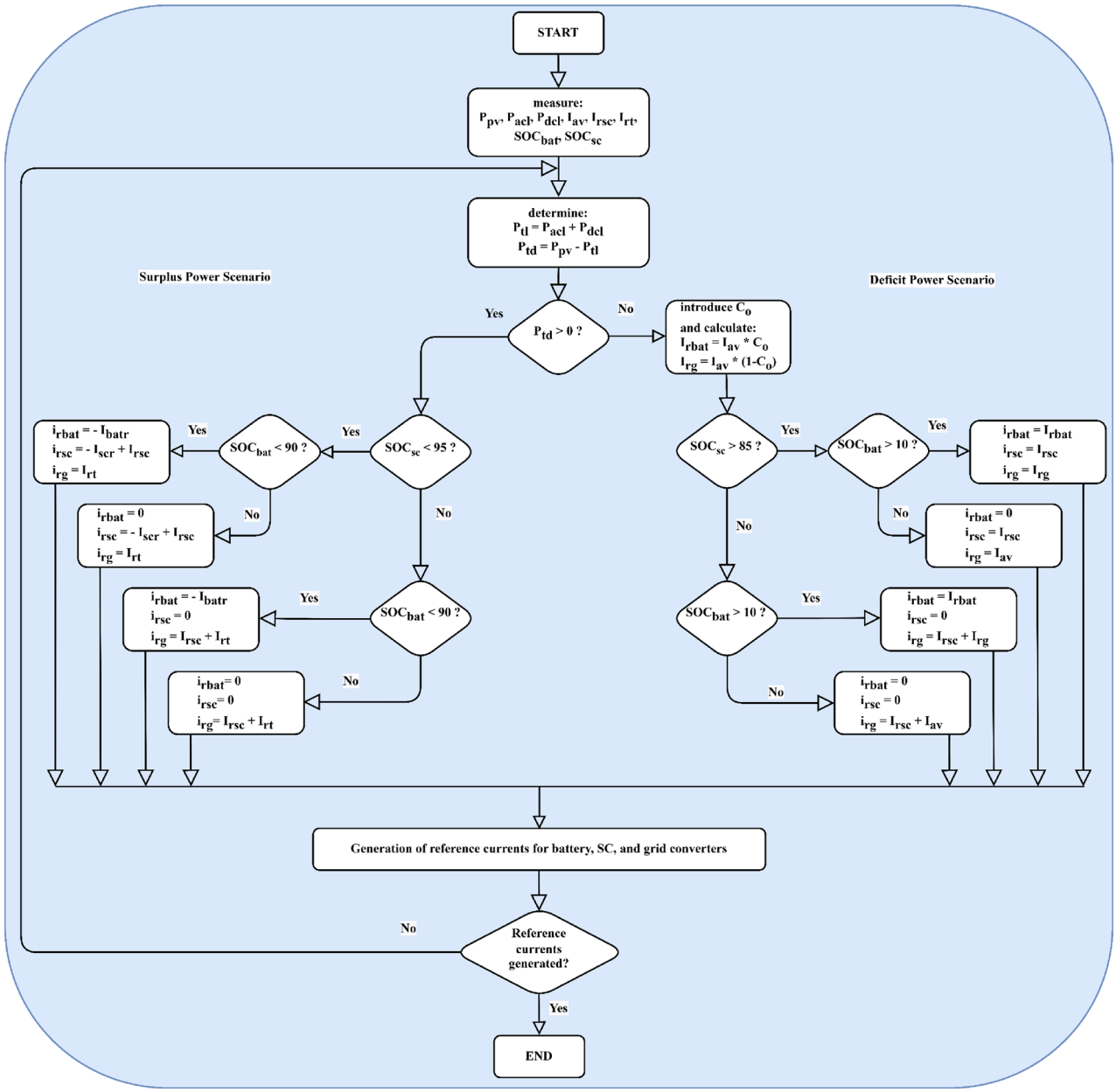

Fig. 5. Flowchart of the proposed MEMS.

Deficit power scenario (DPS)

Figure 8 displays the system's performance under DPS. The total load is kept constant while the irradiance varies following the pattern in Fig. 6 (DPS). SOC_{bat} is set close to its minimum limit (10%) to observe the battery's deep discharge phenomenon. SOC_{sc} remains above its minimum safety limit (85%) because the SC is not likely to have a deep discharge phenomenon. The PV power is kept lower than the total load power.

During the initial phase (0 to 2 s), the battery and the grid compensate for the deficit average PV power following the power allocation coefficient (C_o) scheme.

The irradiance falls at t = 2s and t = 4s, reducing the PV output and causing a DC bus voltage deviation. As a result, the SC responds by meeting transient demand, and the battery and the grid utilize C_o to compensate for the average power needed to sustain the DC bus voltage.

SOC_{bat} achieves its minimum level during the time interval (4 to 5 s), as shown in Fig. 8c. Its current is reduced to zero to prevent the battery from deep discharge (Fig. 8b). The SC responds to this transient occurrence by absorbing the fluctuating power while the grid handles the average power.

At t = 6s, an increase in irradiance amplifies the PV power, resulting in another DC bus voltage deviation. The battery SOC has achieved its minimum level; thus, no action is required. The SC and the grid absorb the fluctuating and steady-state powers to keep the DC bus voltage constant.

Case	SOCs	Actions	Currents
1	$SOC_{bat} < 90\%$ and $SOC_{sc} < 95\%$	- PV supplies the total average power demand; - Surplus PV power is utilized to charge the storage units up to their maximum safety limits, and any remaining surplus power is sent to the grid; - Grid supplies additional power to meet the average demand if necessary; - SC meets the demand for transient power.	$i_{rbat} = -I_{batr}$; $i_{rsc} = -I_{scr} + I_{rsc}$; $i_{rg} = I_{rt}$;
2	$SOC_{bat} > 90\%$ and $SOC_{sc} < 95\%$	- PV supplies the total average power demand; - Surplus PV power is utilized to charge the SC up to its maximum safety limit, and any remaining surplus power is sent to the grid; - Grid meets the demand for average power if necessary; - SC meets the demand for transient power; - No action from the battery.	$i_{rbat} = 0$; $i_{rsc} = -I_{scr} + I_{rsc}$; $i_{rg} = I_{rt}$.
3	$SOC_{bat} < 90\%$ and $SOC_{sc} > 95\%$	- PV supplies the total average power demand; - Surplus PV power is utilized to charge the battery up to its maximum safety limit, and any remaining surplus power is sent to the grid; - Grid meets the transient power demand and, if necessary, provides additional power for average demand; - No action from the SC.	$i_{rbat} = -I_{batr}$; $i_{rsc} = 0$; $i_{rg} = I_{rt} + I_{rsc}$.
4	$SOC_{bat} > 90\%$ and $SOC_{sc} > 95\%$	- PV supplies the total average power demand; - Surplus PV power is sent to the grid; - Grid meets the demand for transient power; - No action from the battery and SC.	$i_{rbat} = 0$; $i_{rsc} = 0$; $i_{rg} = I_{rt} + I_{rsc}$.

Table 2. Surplus power scenario.

Case	SOCs	Actions	Currents
1	$SOC_{bat} > 10\%$ and $SOC_{sc} > 85\%$	- PV supplies its output available average power; - Battery and grid supply the average deficit power demand; - SC handles the transient power demand.	$i_{rbat} = I_{rbat}$; $i_{rsc} = I_{rsc}$; $i_{rg} = I_{rg}$;
2	$SOC_{bat} < 10\%$ and $SOC_{sc} > 85\%$	- PV supplies its output available average power; - Grid provides the average deficit power demand; - SC meets the transient power demand; - No action from the battery.	$i_{rbat} = 0$; $i_{rsc} = I_{rsc}$; $i_{rg} = I_{av}$;
3	$SOC_{bat} > 10\%$ and $SOC_{sc} < 85\%$	- PV supplies its output available average power; - Battery and grid supply the average deficit power demand; - Grid manages the transient power demand; - No action from the SC.	$i_{rbat} = I_{rbat}$; $i_{rsc} = 0$; $i_{rg} = I_{rg} + I_{rsc}$;
4	$SOC_{bat} < 10\%$ and $SOC_{sc} < 85\%$	- PV supplies its output available average power; - Grid supplies the average deficit power demand and meets the transient power demand; - No action from the battery and SC.	$i_{rbat} = 0$; $i_{rsc} = 0$; $i_{rg} = I_{av} + I_{rsc}$;

Table 3. Deficit power scenario.

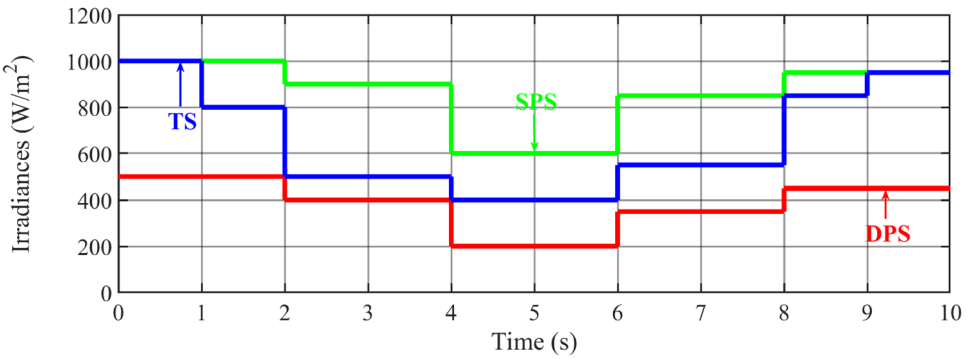

Fig. 6. Irradiance profiles.

Another increase in solar irradiance is seen at t = 8s. Because the battery has hit its minimum safety limit, the SC meets the transient demand, and the grid fulfills the system average requirement to regulate the DC bus voltage.

The SC responds to a sudden rise in DC bus voltage by absorbing the transient power and releasing it in case of a sudden drop. The battery and the grid handle the slow responses. (e), (f), (g), and (h) of Fig. 8 show the

Components	Parameters	Values
PV array	Maximum power	300 Wp
	Open-circuit voltage	44.4 V
	Short-circuit current	8.69 A
Battery	Type	Li-ion
	Capacity	7 Ah
	Nominal voltage	12 V
	No. of batteries in series	20
SC	Capacitance	58 F
	Rated voltage	16 V
	No. of SC in series	20
Converters	PV	L_{pv} = 21 mH
		C_{pv} = 2.92 µF
	Battery	L_{bat} = 23 mH
		C_{bat} = 2.44 µF
	SC	L_{sc} =13 mH
		C_{sc} = 4.02 µF
Grid	Voltage	400 V
	Frequency	50 Hz
Controllers	Voltage loop	K_p = 0.005
		K_i = 5
	Battery	K_p = 0.1
		K_i = 50
	SC	K_p = 0.1
		K_i = 10
LC filter	Inductor	L_f = 230 mH
	Capacitor	C_f = 0.193 µF
DC bus	Voltage	700 V

Table 4. Proposed microgrid configuration parameters.

grid voltages, currents, inverter currents, and the system frequency, respectively. The grid's unity power factor is maintained, and the frequency is regulated.

Transition scenario (TS)

Figure 9 depicts the transition scenario, illustrating two critical transitions: SPS-DPS occurring at t = 2s and DPS-SPS occurring at t = 8s. This scenario showcases the proposed energy management system's performance during shifts from one operational state to another. Throughout these transitions, the total load power remains constant, and solar irradiance fluctuates according to the pattern shown in Fig. 6 (TS).

At t = 2s, the system smoothly transitions from SPS to DPS, with the battery transitioning from charging to discharging mode and the SC ceasing its charging operation.

Similarly, at t = 8s, the system transitions from DPS to SPS, with the battery transitioning from discharging to charging mode and the SC seamlessly shifting from constant SOC to charging mode.

Notably, these transitions occur without supply interruption, ensuring efficient power allocation and maintaining the DC bus voltage at 700 V and the frequency at 50 Hz while sustaining the unity power factor on the grid side.

Moreover, if the grid is unavailable and there is extra power in the system, the PV should operate in power curtailment mode to maintain power balance. On the other hand, if the system power is deficient, load-shedding techniques should be considered to maintain the system's power balance.

Performance analysis

This section analyzes the performance of the proposed method, highlighting the key findings.

Fast DC bus voltage regulation

Fast DC bus voltage regulation refers to the rapid adjustment and stabilization of the voltage level on the DC bus to its desired setpoint (700 V). This is typically achieved within milliseconds, ensuring minimal voltage deviation during transient conditions and maintaining the power system's reliable and efficient operation. The DPS scenario is implemented to analyze the system performance. SOCs are within safe operating limits. Figure 10 shows a zoomed view of the results of a step decrease in solar irradiance at t = 4s. Due to that step decrease in solar irradiance, the PV current decreases. The DC bus voltage deviation caused by this disturbance is compensated

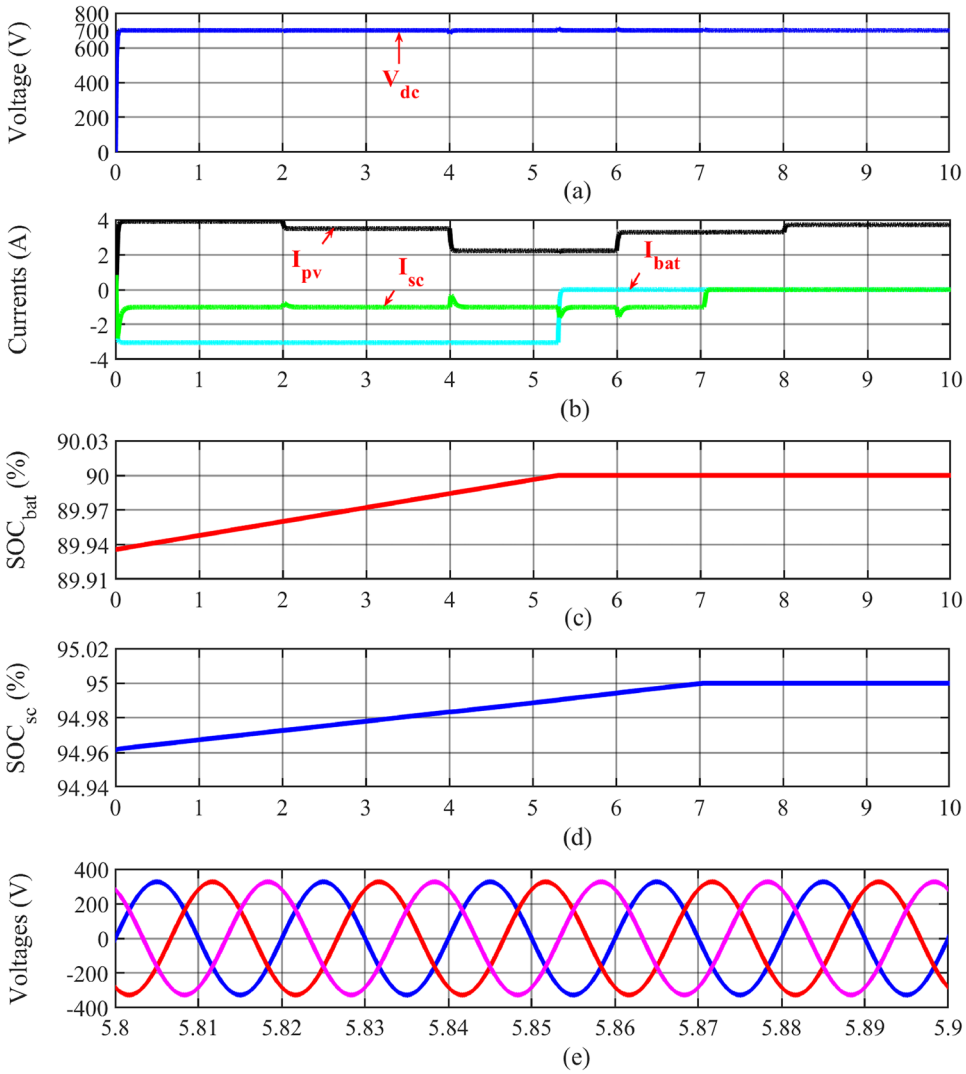

Fig. 7. Results under SPS: (**a**) DC bus voltage; (**b**) PV, battery, and SC currents; (**c**) battery SOC; (**d**) SC SOC; (**e**) grid voltages; (**f**) grid currents; (**g**) inverter currents; (**h**) system frequency; (**i**) powers.

quickly by the SC (transient demand) and slowly by the battery and the grid (average demand). The results show that the grid currents and voltages are in phase, ensuring the unity power factor. In Fig. 10c, the total harmonic distortion measured in the grid current is less than 2%. The system performance indexes are shown in Table 5.

Overall performance analysis

The performance analysis can include many key factors depending on the study's objectives. Based on our research goals, four (4) specific factors are analyzed and compared to previous works: (i) effective power sharing, (ii) stability (voltage, frequency, and transient), (iii) safe operation of storage units, (iv) total harmonics distortion (THD).

Effective power-sharing refers to the optimal distribution of generated power among various energy sources and loads, maintaining the balance between generation and consumption and ensuring stable and reliable operation across all operating scenarios. It is essential for the seamless functioning of DC microgrids, especially when integrating multiple distributed energy resources.

Stability refers to the system's ability to maintain a steady state and operate reliably under normal and abnormal conditions. Stability ensures that the microgrid can sustain its voltage, frequency, and overall power quality within acceptable limits when subjected to various disturbances, such as changes in load, generation fluctuations, and other transient events. It shows the robustness of the control method. In our context, voltage, frequency, and transient stability are considered for the analysis.

Safely operating storage units involves preventing their premature degradation. The battery and SC should operate within safe limits, and high currents should not be allocated to the battery. These measures can potentially extend the lifetime of the storage units.

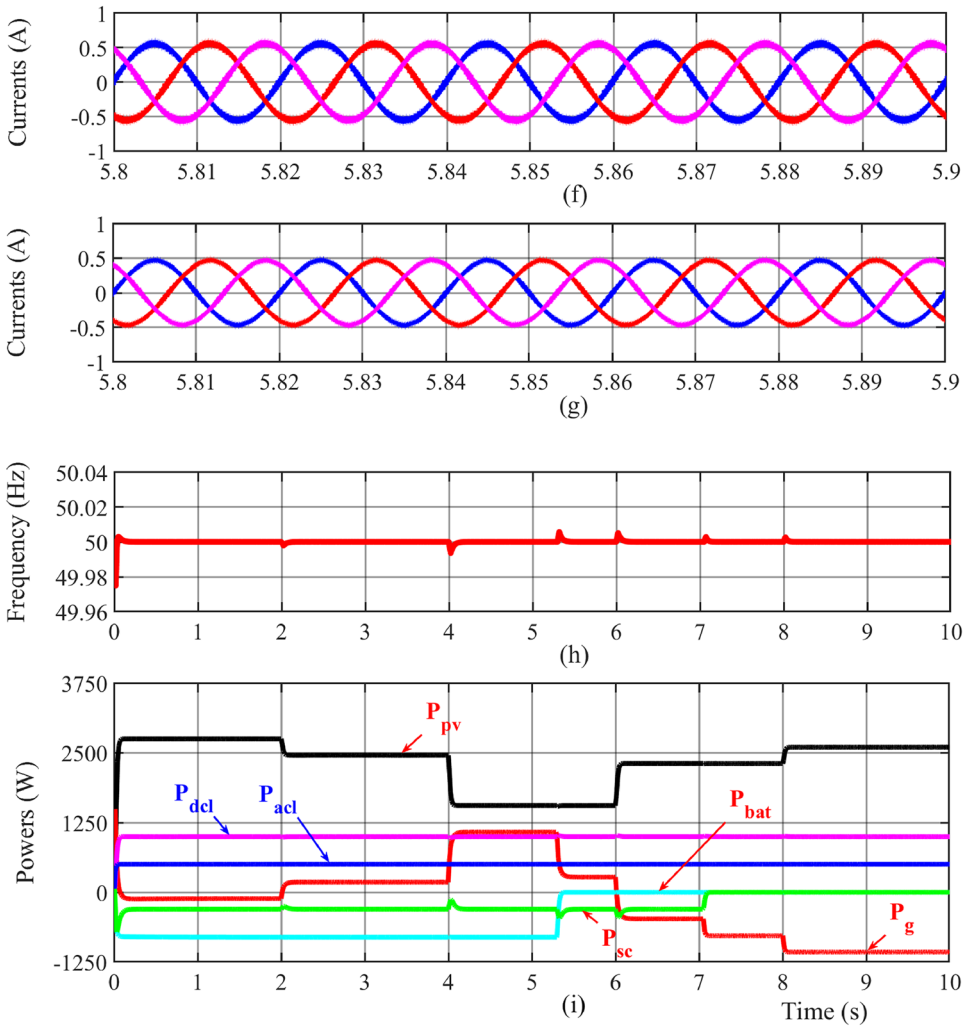

Fig. 7. (continued)

Total harmonic distortion (THD) is a crucial power quality metric that quantifies the level of distortion in a signal caused by harmonics. High THD can result in inefficiencies, overheating, and potential damage to electrical systems. Hence, maintaining low THD is vital for system power quality, reliability, and equipment longevity.

Table 6 provides a performance comparison between the proposed method and previous studies based on the four (4) analyzed factors.

Based on the results in Figs. 7, 8, 9 and 10, the proposed energy management scheme successfully shares power between sources and loads while maintaining energy balance. Additionally, it ensures that voltage and frequency are kept within acceptable ranges, storage units are safely operated, and THD is maintained very low. Moreover, the method's simplicity enhances its suitability for real-world applications, making it a practical solution for DC microgrid systems. It can be concluded that the proposed energy management scheme is highly effective in several key areas. These outcomes indicate that the method is reliable, efficient, and capable of optimizing the overall performance and stability of DC microgrids. Our proposed method overtakes the drawbacks of existing methods. Future works will include real-world implementation and control involving multiple renewable energy sources.

Conclusion

This research presents an effective energy management technique for a grid-interactive microgrid and battery-SC HESS. The proposed technique is analyzed under different scenarios with changes in loads and generation. The findings reveal that the proposed energy management approach facilitates adequate power management, reduces battery stress, regulates the DC bus voltage, safely operates energy storage elements, and ensures a smooth transition between different scenarios, regardless of operating conditions. In addition to its simplicity, the method has also shown an improvement in power quality features by maintaining a unity power factor for the AC grid. Future research will focus on practical implementation and control involving multiple renewable energy sources.

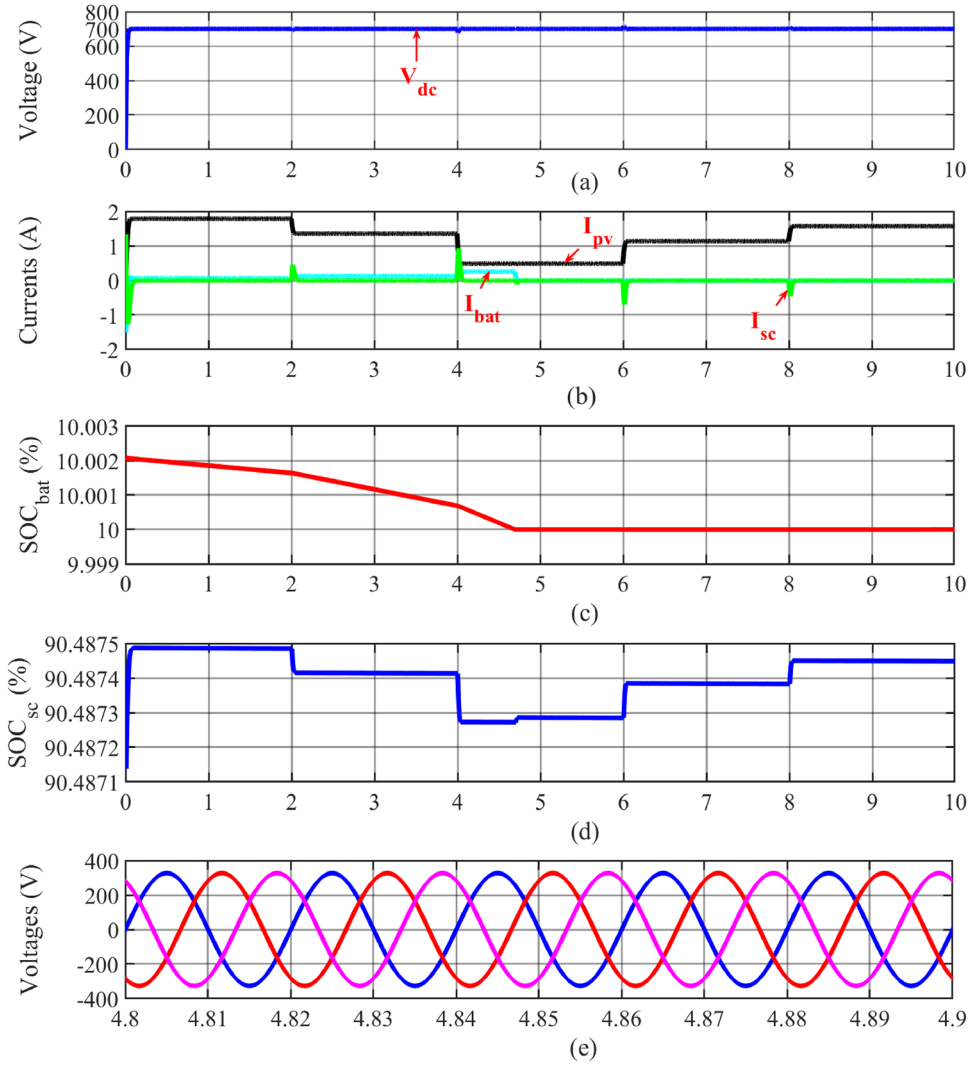

Fig. 8. Results under DPS: (**a**) DC bus voltage; (**b**) PV, battery, and SC currents; (**c**) battery SOC; (**d**) SC SOC; (**e**) grid voltages; (**f**) grid currents; (**g**) inverter currents; (**h**) system frequency; (**i**) powers.

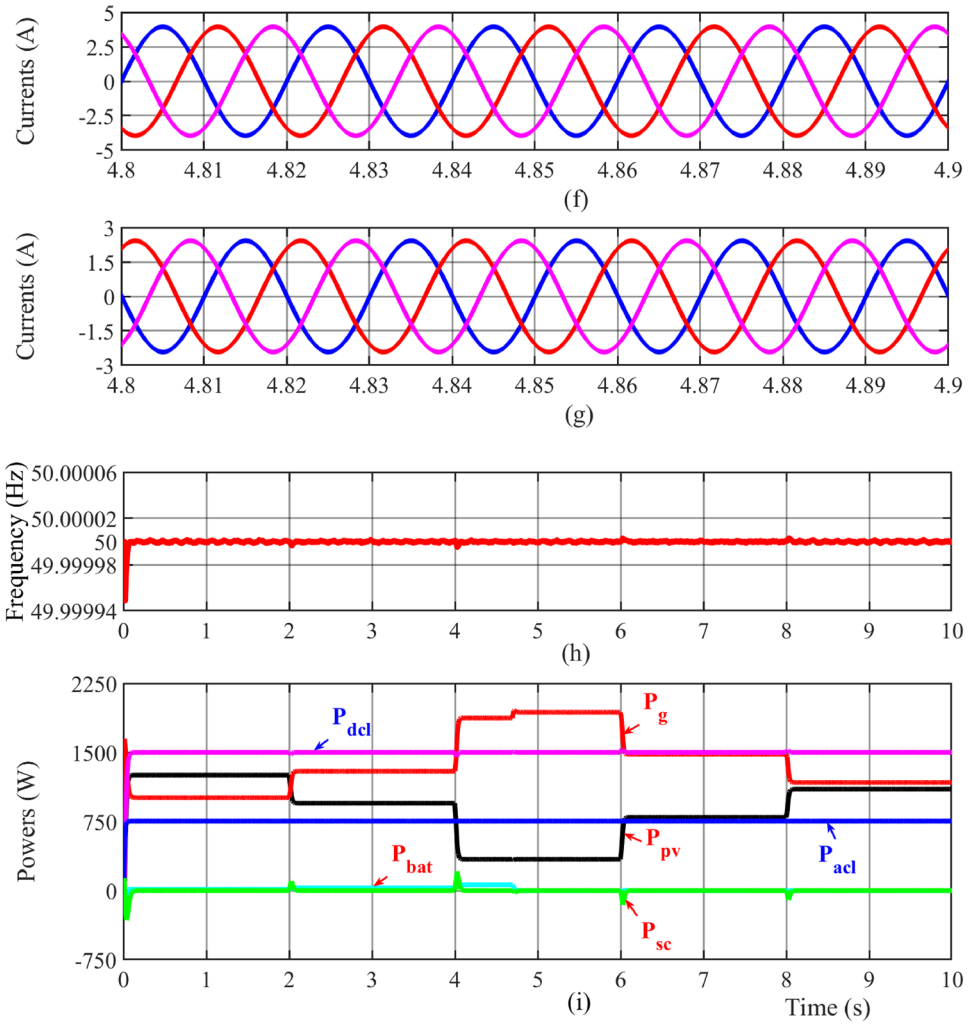

Fig. 8. (continued)

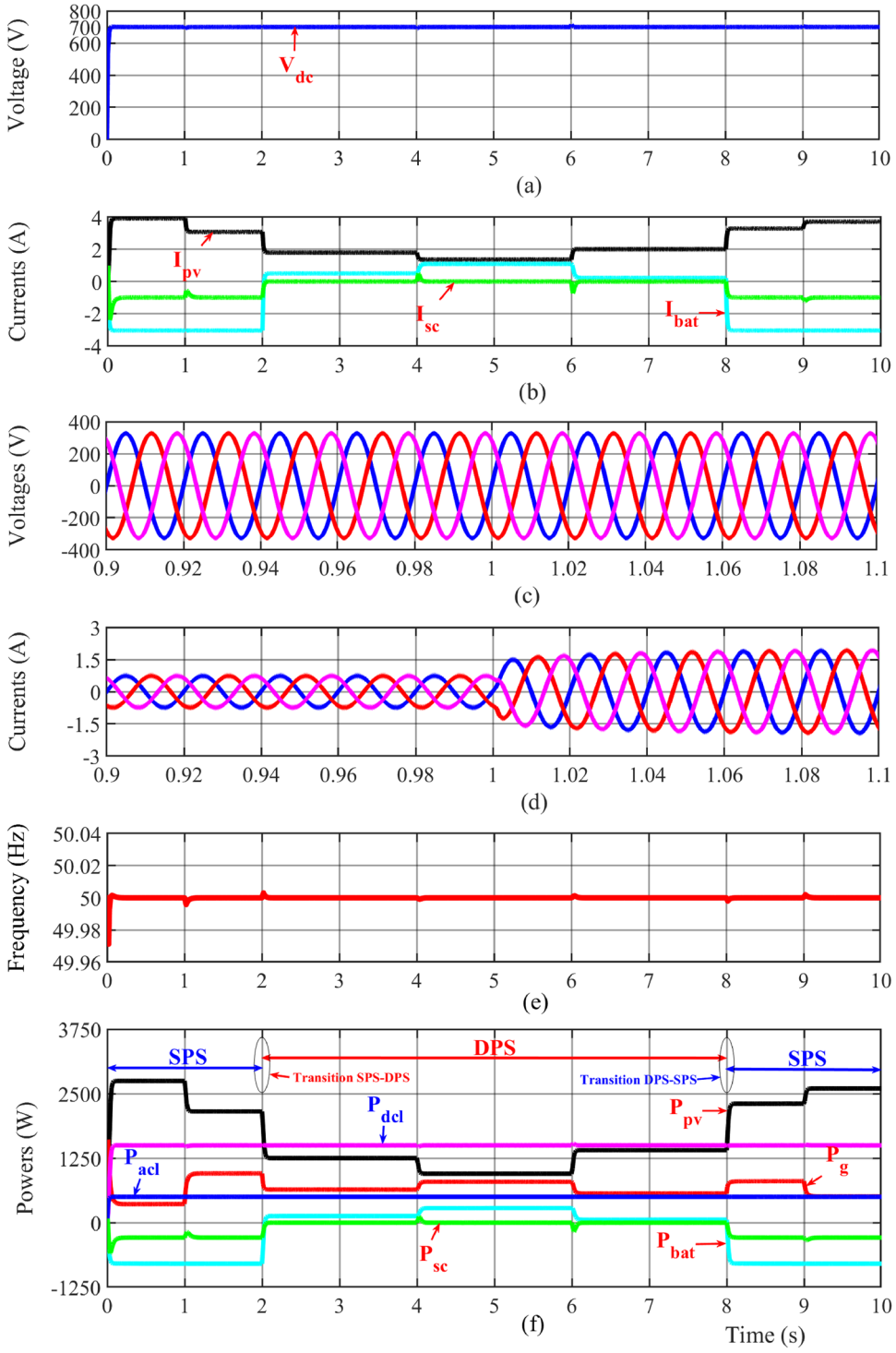

Fig. 9. Results under TS: (**a**) DC bus voltage; (**b**) PV, battery, and SC currents; (**c**) grid voltages; (**d**) grid currents; (**e**) system frequency; (**f**) powers.

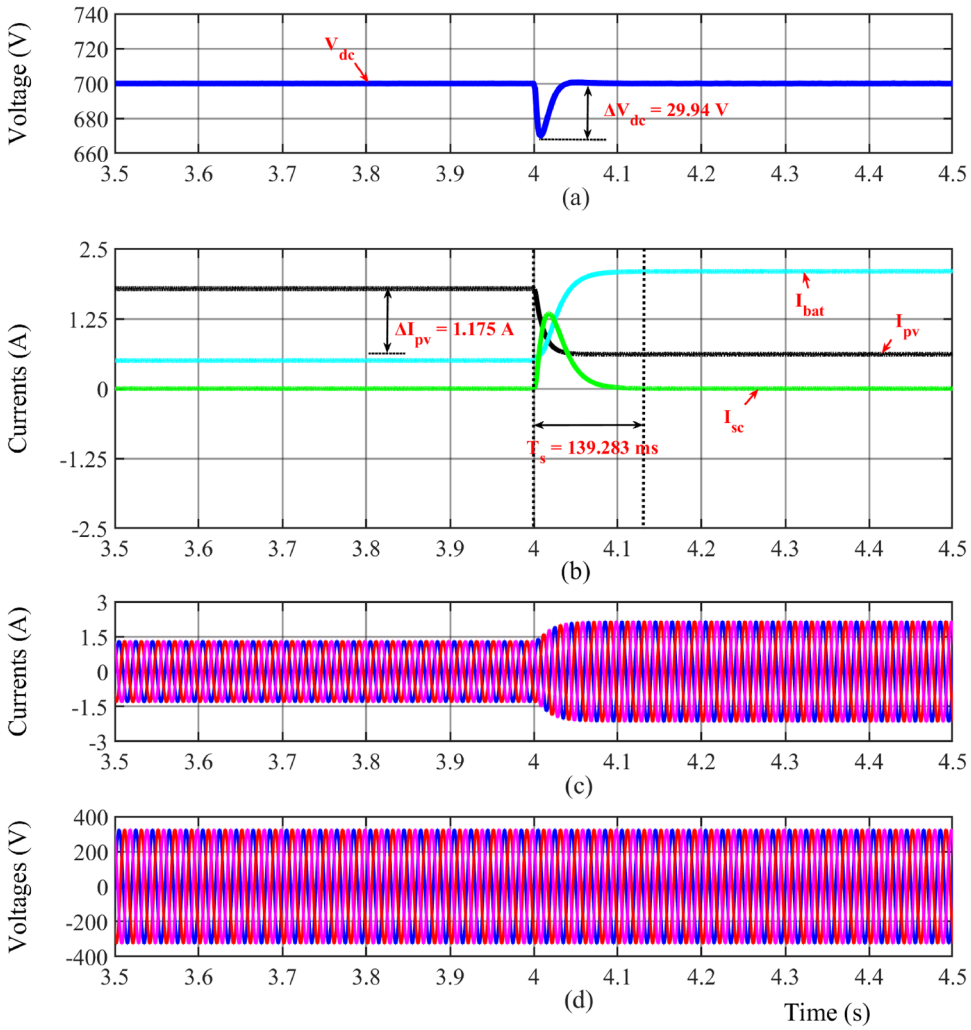

Fig. 10. Zoomed view of transient performance: (**a**) DC bus voltage; (**b**) PV, battery, and SC currents; (**c**) grid currents; (**d**) grid voltages.

Performance index	Value
Average voltage (V_{dc})	699.3 V
Solar irradiance variation	270 W/m^2
PV current variation (ΔI_{pv})	1. 175 A
Peak voltage overshoot, PO = ($\Delta V_{dc}/V_{dc}$)*100	4.2%
Settling time (T_s)	139.283 ms
Overall efficiency, G = V_{dc}/V_{dcr}	0.999

Table 5. System transient performance.

Metric		[20]	[23]	Proposed
Effective power-sharing		✓	✓	✓
Stability	Voltage	✓	✓	✓
	Frequency	–	–	✓
	Transient	✓	✓	✓
Storage units' safe operation	Battery working within safety limits	✓	✓	✓
	Avoidance of high currents in the battery	✓	✖	✓
	SC working within safety limits	✓	✓	✓
THD		< 7%	–	< 2%

Table 6. Performance comparison.

Data availability

The data supporting the findings of this study are available in the paper.

Received: 23 May 2024; Accepted: 19 August 2024
Published online: 31 August 2024

References

1. Elshurafa, A. M. The value of storage in electricity generation: A qualitative and quantitative review. *J. Energy Stor.* **32**, 101872. https://doi.org/10.1016/j.est.2020.101872 (2020).
2. Farivar, G. G. et al. Grid-connected energy storage systems: State-of-the-art and emerging technologies. *Proc. IEEE* **111**(4), 397–420. https://doi.org/10.1109/JPROC.2022.3183289 (2023).
3. Zarate-Perez, E., Rosales-Asensio, E., González-Martínez, A., de Simón-Martín, M. & Colmenar-Santos, A. Battery energy storage performance in microgrids: A scientific mapping perspective. *Energy Rep.* **8**, 259–268. https://doi.org/10.1016/j.egyr.2022.06.116 (2022).
4. Salman, U. T., Al-Ismail, F. S. & Khalid, M. Optimal sizing of battery energy storage for grid-connected and isolated wind-penetrated microgrid. *IEEE Access* **8**, 91129–91138. https://doi.org/10.1109/ACCESS.2020.2992654 (2020).
5. Alshehri, J., Khalid, M. & Alzahrani, A. An intelligent battery energy storage-based controller for power quality improvement in microgrids. *Energies* **12**(11), 2112. https://doi.org/10.3390/en12112112 (2019).
6. Li, J. Design and real-time test of a hybrid energy storage system in the microgrid with the benefit of improving the battery lifetime. *Appl. Energy* **218**, 470–478. https://doi.org/10.1016/j.apenergy.2018.01.096 (2018).
7. Sutikno, T., Arsadiando, W., Wangsupphaphol, A., Yudhana, A. & Facta, M. A review of recent advances on hybrid energy storage system for solar photovoltaics power generation. *IEEE Access* **10**, 42346–42364. https://doi.org/10.1109/ACCESS.2022.3165798 (2022).
8. Atawi, I. E., Al-Shetwi, A. Q., Magableh, A. M. & Albalawi, O. H. Recent advances in hybrid energy storage system integrated renewable power generation: Configuration, control, applications, and future directions. *Batteries* **9**(1), 29. https://doi.org/10.3390/batteries9010029 (2023).
9. Hajiaghasi, S., Salemnia, A. & Hamzeh, M. Hybrid energy storage system for microgrids applications: A review. *J. Energy Stor.* **21**, 543–570. https://doi.org/10.1016/j.est.2018.12.017 (2019).
10. Nguyen, B. H., German, R., Trovao, J. P. F. & Bouscayrol, A. Real-time energy management of battery/supercapacitor electric vehicles based on an adaptation of Pontryagin's minimum principle. *IEEE Trans. Veh. Technol.* **68**(1), 203–212. https://doi.org/10.1109/TVT.2018.2881057 (2019).
11. Hemmati, R. & Saboori, H. Emergence of hybrid energy storage systems in renewable energy and transport applications – A review. *Renew. Sustain. Energy Rev.* **65**, 11–23. https://doi.org/10.1016/j.rser.2016.06.029 (2016).
12. Ruan, J., Song, Q. & Yang, W. The application of hybrid energy storage system with electrified continuously variable transmission in battery electric vehicle. *Energy* **183**, 315–330. https://doi.org/10.1016/j.energy.2019.06.095 (2019).
13. Arunkumar, C. R., Manthati, U. B. & Srinivas, P. Accurate modelling and analysis of battery–supercapacitor hybrid energy storage system in DC microgrid systems. *Energy Syst.* **13**(4), 1055–1073. https://doi.org/10.1007/s12667-021-00467-3 (2022).
14. Jing, W., Lai, H., Wong, C. & Wong, M. L. D. Battery-supercapacitor hybrid energy storage system in standalone DC microgrids: A review. *IET Renew. Power Gen.* **11**(4), 461–469. https://doi.org/10.1049/iet-rpg.2016.0500 (2017).
15. Babu, T. S. et al. A comprehensive review of hybrid energy storage systems: Converter topologies, control strategies, and future prospects. *IEEE Access* **8**, 148702–148721. https://doi.org/10.1109/ACCESS.2020.3015919 (2020).
16. Ramos, G. A. & Costa-Castelló, R. Energy management strategies for hybrid energy storage systems based on filter control: Analysis and comparison. *Electronics* **11**(10), 1631. https://doi.org/10.3390/electronics11101631 (2022).
17. Zizoui, M. Z. et al. Photovoltaic-battery-ultracapacitor-diesel hybrid generation system for mobile hospital energy supply. *Electronics* **11**(3), 390. https://doi.org/10.3390/electronics11030390 (2022).
18. Pannala, S., Patari, N., Srivastava, A. K. & Padhy, N. P. Effective control and management scheme for isolated and grid connected DC microgrid. *IEEE Trans. Ind. Appl.* **56**(6), 6767–6780. https://doi.org/10.1109/TIA.2020.3015819 (2020).
19. Oriti, G., Anglani, N. & Julian, A. L. Hybrid energy storage control in a remote military microgrid with improved supercapacitor utilization and sensitivity analysis. *IEEE Trans. Ind. Appl.* **55**(5), 5099–5108. https://doi.org/10.1109/TIA.2019.2923380 (2019).
20. Manandhar, U. Energy management and control for grid connected hybrid energy storage system under different operating modes. *IEEE Trans. Smart Grid* **10**(2), 1626–1636. https://doi.org/10.1109/TSG.2017.2773643 (2019).
21. Elmorshedy, M. F., Elkadeem, M., Kotb, K. M., Taha, I. B. & Mazzeo, D. Optimal design and energy management of an isolated fully renewable energy system integrating batteries and supercapacitors. *Energy Convers. Manag.* **245**, 114584. https://doi.org/10.1016/j.enconman.2021.114584 (2021).
22. Aktaş, A. & Kırçiçek, Y. A novel optimal energy management strategy for offshore wind/marine current/battery/ultracapacitor hybrid renewable energy system. *Energy* **199**, 117425. https://doi.org/10.1016/j.energy.2020.117425 (2020).
23. Abadi, S. A. G. K. & Bidram, A. A distributed rule-based power management strategy in a photovoltaic/hybrid energy storage based on an active compensation filtering technique. *IET Renew. Power Gen.* **15**(15), 3688–3703. https://doi.org/10.1049/rpg2.12263 (2021).

24. Faria, J., Pombo, J., Calado, M. & Mariano, S. Power management control strategy based on artificial neural networks for standalone PV applications with a hybrid energy storage system. *Energies* **12**(5), 902. https://doi.org/10.3390/en12050902 (2019).
25. Singh, P. & Lather, J. S. Accurate power-sharing, voltage regulation, and SOC regulation for LVDC microgrid with hybrid energy storage system using artificial neural network. *Int. J. Green Energy* **17**(12), 756–769. https://doi.org/10.1080/15435075.2020.1798767 (2020).
26. Ramoul, J., Chemali, E., Dorn-Gomba, L. & Emadi, A. A neural network energy management controller applied to a hybrid energy storage system using multi-source inverter. *2018 IEEE Energy Convers. Congress Expos. (ECCE)* https://doi.org/10.1109/ECCE.2018.8558326 (2018).
27. Chen, H., Xiong, R., Lin, C. & Shen, W. Model predictive control based real-time energy management for hybrid energy storage system. *CSEE J. Power Energy Syst.* **7**(4), 862–874. https://doi.org/10.17775/CSEEJPES.2020.02180 (2021).
28. Nair, U. R. & Costa-Castello, R. A model predictive control-based energy management scheme for hybrid storage system in islanded microgrids. *IEEE Access* **8**, 97809–97822. https://doi.org/10.1109/ACCESS.2020.2996434 (2020).
29. Abadi, S. G. K., Habibi, S. I., Khalili, T. & Bidram, A. A model predictive control strategy for performance improvement of hybrid energy storage systems in DC microgrids. *IEEE Access* **10**, 25400–25421. https://doi.org/10.1109/access.2022.3155668 (2022).
30. Fallah Ghavidel, H. & Mousavi-G, S. M. Modeling analysis, control, and type-2 fuzzy energy management strategy of hybrid fuel cell-battery-supercapacitor systems. *J. Energy Stor.* **51**, 104456. https://doi.org/10.1016/j.est.2022.104456 (2022).
31. Zahedi, R. & Ardehali, M. Power management for storage mechanisms including battery, supercapacitor, and hydrogen of autonomous hybrid green power system utilizing multiple optimally-designed fuzzy logic controllers. *Energy* **204**, 117935. https://doi.org/10.1016/j.energy.2020.117935 (2020).
32. Zhao, Z. H. Improved fuzzy logic control-based energy management strategy for hybrid power system of FC/PV/battery/SC on tourist ship. *Int. J. Hydrogen Energy* **47**(16), 9719–9734. https://doi.org/10.1016/j.ijhydene.2022.01.040 (2022).
33. Ilyas, A., Ayyub, M., Khan, M. R., Jain, A. & Husain, M. A. Realisation of incremental conductance the MPPT algorithm for a solar photovoltaic system. *Int. J. Ambient Energy* **39**(8), 873–884. https://doi.org/10.1080/01430750.2017.1354322 (2018).

Author contributions

All authors contributed to the study, design, simulation, and manuscript writing and read and approved the final manuscript.

Competing interests

The authors declare no competing interests.

Additional information

Correspondence and requests for materials should be addressed to Y.K.

Reprints and permissions information is available at www.nature.com/reprints.

Publisher's note Springer Nature remains neutral with regard to jurisdictional claims in published maps and institutional affiliations.